

*Full Length Research Paper*

# Distribution of turbulence statistics in open-channel flow

Ömer KÖSE

Civil Engineering Department, Aksaray University, Aksaray, Turkey. E-mail: omerkose@aksaray.edu.tr.

Accepted 14 June, 2011

**Turbulence is ubiquitous in most environmental flows. Therefore, highly resolved measurement of turbulent quantities is one of the challenges in hydraulics. As turbulence is a multi-scale physical phenomenon, the measurement resolution should be sufficient to capture all these scales. Therefore, research on turbulent flow gained momentum after the introduction of high-resolution measurement devices such as Laser Doppler Velocimeter (LDV) and Acoustic Doppler Velocimeter (ADV). In this study, a set of experiments were conducted by using ADV to measure the flow turbulence in a trapezoidal open channel on rough bed which is commonly observed in a typical riverine environment. In the experiments, vertical distribution of the turbulent quantities was investigated. The experiments are conducted by using a four component ADV with maximum sampling frequency of 200 Hz. Measured velocity data are filtered to eliminate the artifacts due to spikes, low correlation and SNR velocity values. The filtered data are then analyzed to obtain the statistical parameters that characterize the flow turbulence in the water column ranging from the smallest scale to integral length scale.**

**Key words:** Turbulence, open channel, spectral analysis.

## INTRODUCTION

Acoustic doppler velocimeter (ADV) were introduced in the U.S Army Engineer Waterways Experiment Station (WES) in 1992 to satisfy the need for an accurate current meter that can measure three dimensional (3D) dynamic flow in physical models (Lohrmann et al., 1994). ADV's are intrusive devices so minimum disturbance to the flow is very important for accurate measurement. Since from its first use, ADV's found widespread use in river engineering and turbulent open channel flows. Detailed working principles and the limitations of ADV's have been discussed (Kraus et al., 1995; Lhermitte and Lemmin, 1994; Lohrmann et al., 1995; Zedel et al., 1996). Various applications using ADV's on open channel and river studies are conducted by Voulgaris and Trowbridge (1998), Lane et al. (1998), Lopez and Garcia (1999), Finelli et al. (1999), Synder and Castro (1999), Nikora and Goring (2000), Belanger et al. (2000), Garcia et al. (2005); Carollo et al. (2005); Tricito and Hotchkiss (2005), Blanckaert and Lemmin (2006) and Lacey and Roy (2008). The raw data collected by ADV's cannot be used directly because data contain noises, spikes, thus must be filtered. Mainly, two types of noises exist: Doppler Noise and Spikes. Doppler noise is associated with the measurement process itself. The term is an inherent part

of all Doppler-based volume backscatter system (Lohrmann et al., 1995). Another problem with ADV's is spikes caused by aliasing of the Doppler signal if the phase shift between the outgoing and incoming pulse lies outside the range between  $-180$  and  $+180^\circ$  and there is ambiguity causing a spike in the record. Such a situation can occur when the flow velocity exceeds the preset velocity range or when there is contamination from previous pulses reflected from the boundaries of complex geometries (e.g., cobbles on a stream) (Goring and Nikora, 2002). Effective filtering methods are proposed to filter ADV velocity time series such as Voulgaris and Trowbridge (1998), Blanckaert and Lemmin (2006), Garcia et al. (2005), Wahl (2000), Goring and Nikora (2002) and Cea et al. (2007). Here to filter raw velocity time series, the methods proposed in Goring and Nikora (2002) are applied. After velocity time series are filtered, their statistical characteristics are obtained, and then distribution of mean velocity profile is checked.

In this study, a trial was made to obtain much data very close to the bed. Using these data, the sizes of coherent structures were investigated. Distribution of turbulence intensity, Reynolds stresses for three velocity components, integral time scales, integral length scales and



**Figure 1.** ADV, frame and the flow channel.

turbulence kinetic energies are calculated, interpreted along water depth and compared with the other studies cited in the literature. Distribution of spectral density function is also analyzed especially very close to the bed. The aim of the study is especially to reach a better understanding of the distribution of turbulence statistics, and sizes of coherent structures along vertically in an open channel.

#### EXPERIMENTAL SETUP AND MEASUREMENTS

Measurements are conducted at the center of a trapezoidal channel (Mosalman et al., 2011). As shown in Figure 1, to avoid boundary layer effect from the sides of the channel, the sensor was ensured to be sufficiently away from the legs of the frame so that the wakes formed around the legs do not contaminate the measurements. The depth is constant and measured as 22.36 cm. 46 data points along the water column are selected. The specifications of the ADV in the experiments range:  $\pm 0.01$ , 0.1, 0.3, 1, 2 and 4 m/s. Maximum output sampling rate was 200 Hz. The accuracy is  $\pm 0.5\%$  of the measured values, that is,  $\pm 1$  mm/s. sampling volume is 5 cm from the probe, diameter of the sampling volume is 6 mm, and height is 3 to 15 mm (user selectable). Doppler noise uncertainty at 25 Hz is 1% of velocity range. ADV is mounted onto a frame that has the mobility in all three directions. A ruler is attached into the frame to adjust ADV in all directions in the precision of millimeters. In addition to the ruler, the distance from the bed is ensured by the distance sensor

of the ADV. The data is sampled with a frequency of 100 Hz. During the experiments, the increase in the sampling frequency, leads to an increase in the Doppler noise level in the form of emphasized spikes. From preliminary measurements, it is observed that 1 min sampling time is satisfactory for each measurement point (Tricito and Hotchkiss, 2005).

#### FILTERING AND STATISTICAL CHARACTERISTICS OF DATA

The measurements from ADV are recorded to a computer. Prior to filtering of the raw data, two important parameters are the signal-to-noise-ratio (SNR) and the correlation (COR) parameters. The criteria for SNR are taken as 15, and COR criteria are applied as 70%. Firstly, low correlation or SNR scores are eliminated.

The unfiltered data will not be normally distributed due to the effect of the spikes, (outliers) which is also observed in the current set of measurements. The assumption of normal distribution, applies to the actual velocities that we try to measure. After the removal of the outliers, the final result looks closely to normal distribution which is given in Figure 2. To filter velocity time series for each component, phase-space filter algorithm (Goring and Nikora, 2002) is used.

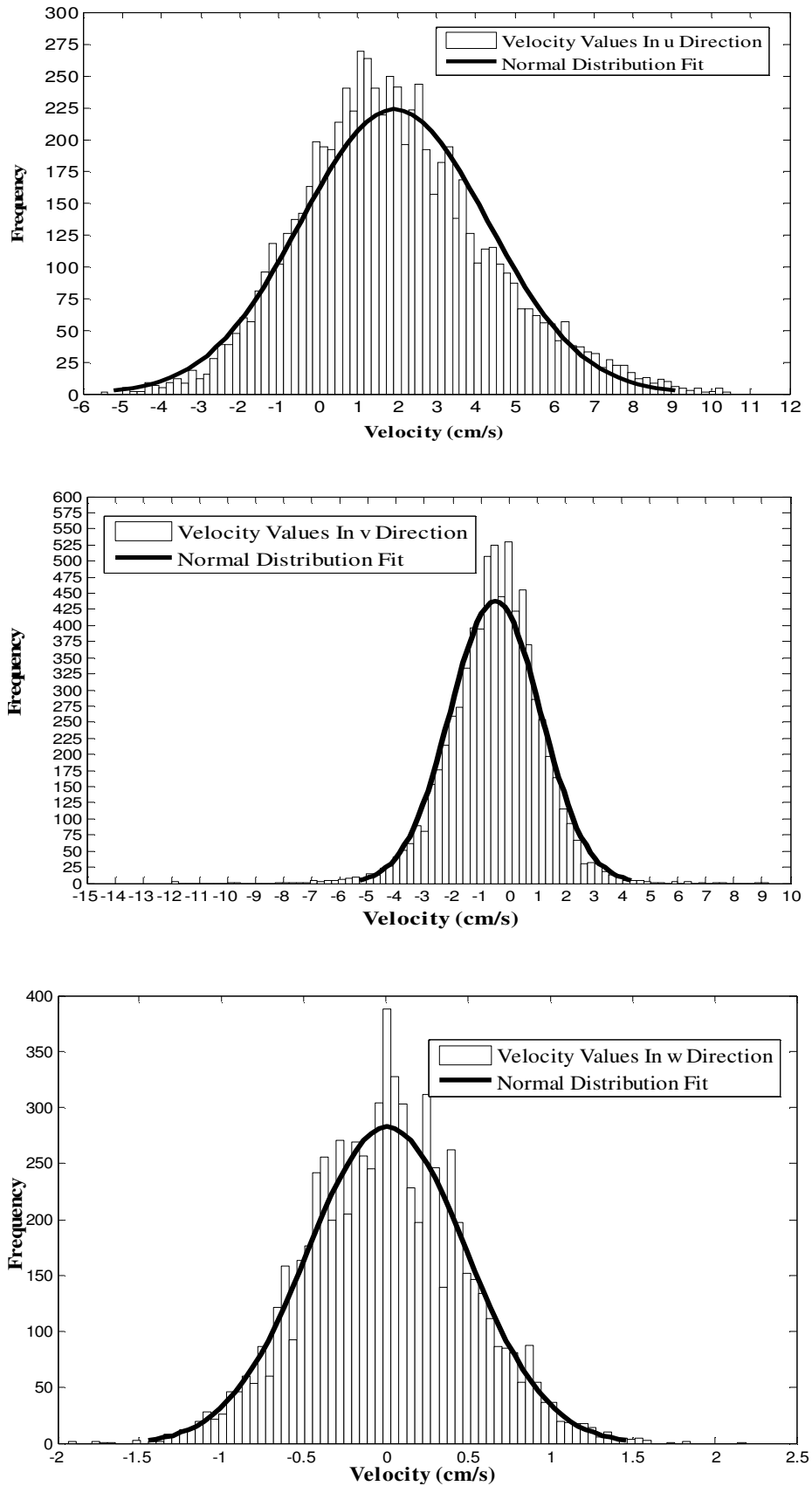


**Figure 2.** Histograms and normal distribution fits for velocity values at point 3 for x, y, z directions.

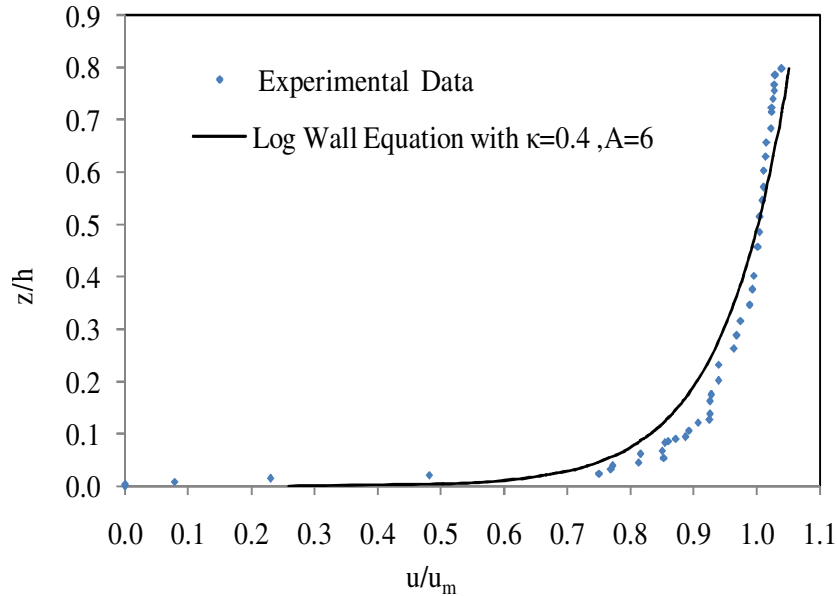


Figure 3. Vertical distribution of mean velocity profile.

This method is an effective tool to detect and replace spikes. After filtering, the histogram of the velocity time series are drawn and given in Figure 2. As seen in the aforementioned figure, the distribution of velocity time series becomes very close to the normal distribution.

Turbulence is three dimensional in nature, and therefore all three components of velocity data are sampled with 0.01 s of time intervals, the fluctuating velocities are calculated by subtraction of the mean value of the velocity components, which is denoted by an over bar:

$$u' = U - \bar{U}, v' = V - \bar{V}, w' = W - \bar{W} \quad (1)$$

The flow in the trapezoidal channel is assumed to be uniform but as seen from the Histograms  $\bar{V}$  and  $\bar{W}$  values are close to zero but not exactly zero. The situation is attributed to the secondary currents. Turbulence statistics are: Ensemble-averaged velocity in x direction at time t

$$\bar{U} = \frac{1}{N} \sum_{i=1}^N U(i) \quad (2)$$

Mean square difference from the time-averaged velocity that is the variance is given as follows:

$$s^2 = \overline{u' u'} \quad (3)$$

The square root of the variance gives the turbulent intensity (Bombar et al., 2010).

$$s = (\overline{u'^2})^{1/2} \quad (4)$$

### Mean longitudinal velocity distribution

Vertical distribution of mean stream wise velocity is to follow the log law at smooth and fully rough open channels between  $z/h = [0, 0.2]$  (Nezu and Rodi, 1986). The measurement points are located close to the bottom wall within this layer to capture the characteristics of the log-law which can be given as follows:

$$\frac{\bar{U}}{u_*} = \frac{1}{\kappa} \ln \frac{z u_*}{\nu} + A \quad (5)$$

In Equation 5,  $\bar{U}$  is the mean velocity,  $u_*$  is the friction velocity,  $\kappa$  is the von Karman constant,  $\nu$  is the kinematic viscosity and  $A$  is an integration constant. Through experimental observations, Nikuradse  $\kappa$  and  $A$  values are obtained as 0.4 and 5.5, respectively. In Figure 3, observed mean velocity profile is given with as solid line. The velocity profile obtained through Equation 5 with  $\kappa$  and  $A$  values as 0.4 and 6 are given with a dashed line. The values given are the best fit values for  $\kappa$  and  $A$ . The differentiation of Equation (5) gives us the following relation:

$$u_* = \frac{\kappa}{\ln(10)} \frac{d\bar{U}}{d(\log z)} \quad (6)$$

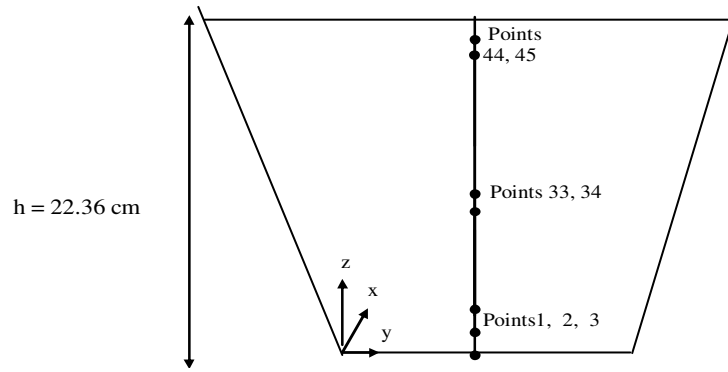


Figure 4. Measurement points.

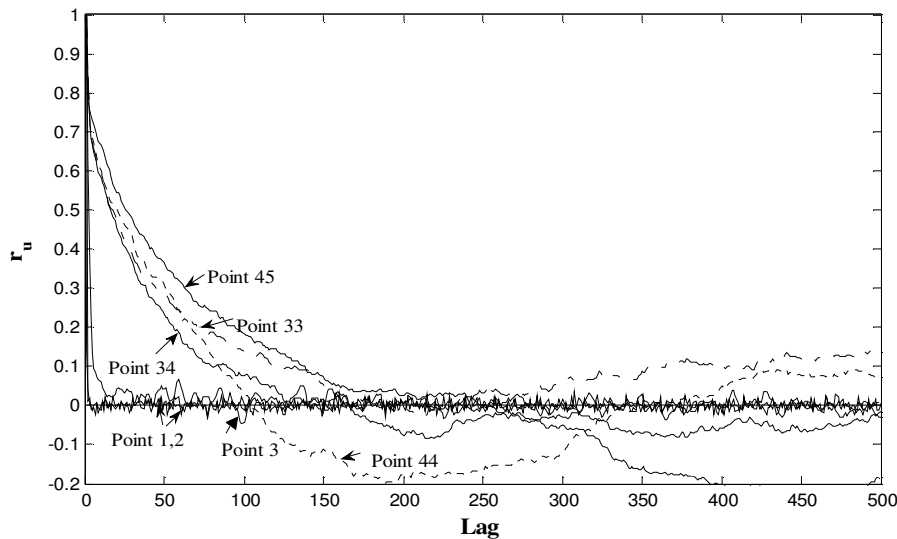


Figure 5. Autocorrelation coefficients for points 1, 2, 3, 33, 34, 44 and 45 for u component.

If the velocity versus the normalized depth is plotted in logarithmic scale, the slope gives the value of the frictional velocity. By using Equation 6, the frictional velocity is found to be 0.92 cm/s.

**Analyses of autocorrelation function, integral time and length scales**

Autocorrelation function describes the correlation between the consecutive values of the time series. Generally it is used to check the dependency in time series data for various research fields; here it is used to interpret a physical event. Utilizing the Taylor’s frozen turbulence hypothesis, the autocorrelation of the velocity fluctuations becomes useful tool for finding repeating patterns such as the presence of a periodic circulating structure. In this study, autocorrelation analysis is applied to detect dependent and coherent structures such as

eddies. The behavior of the autocorrelation function of the measurement points very close to the bed, in the middle, and close to the surface are investigated and interpreted for all velocity components. Representative points are given in Figure 4.

Using autocorrelation functions, integral time and integral length scales are calculated for each direction. The normalized autocorrelation function in the stream wise direction can be given as in the following that is repeated for all the directions,

$$r_{uu}(\Delta t) = \frac{\overline{u'(t)u'(t + \Delta t)}}{\overline{u'(t)u'(t)}} \tag{7}$$

The auto-correlation function versus time lags ( $\Delta t$ ), which is  $\Delta t = 0.01$  s, is given in Figures 5 to 7. In the aforementioned figures the auto-correlation functions are

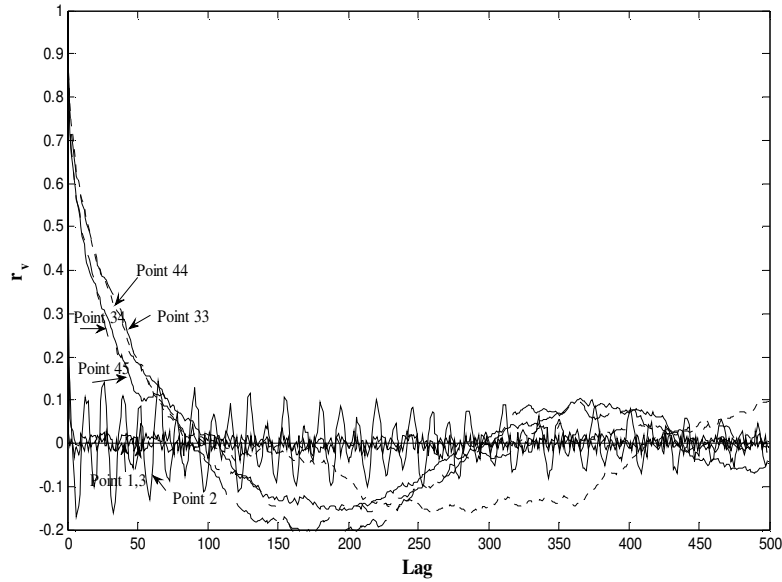


**Figure 6.** Autocorrelation coefficients for points 1, 2, 3, 33, 34, 44, 45 for v component.

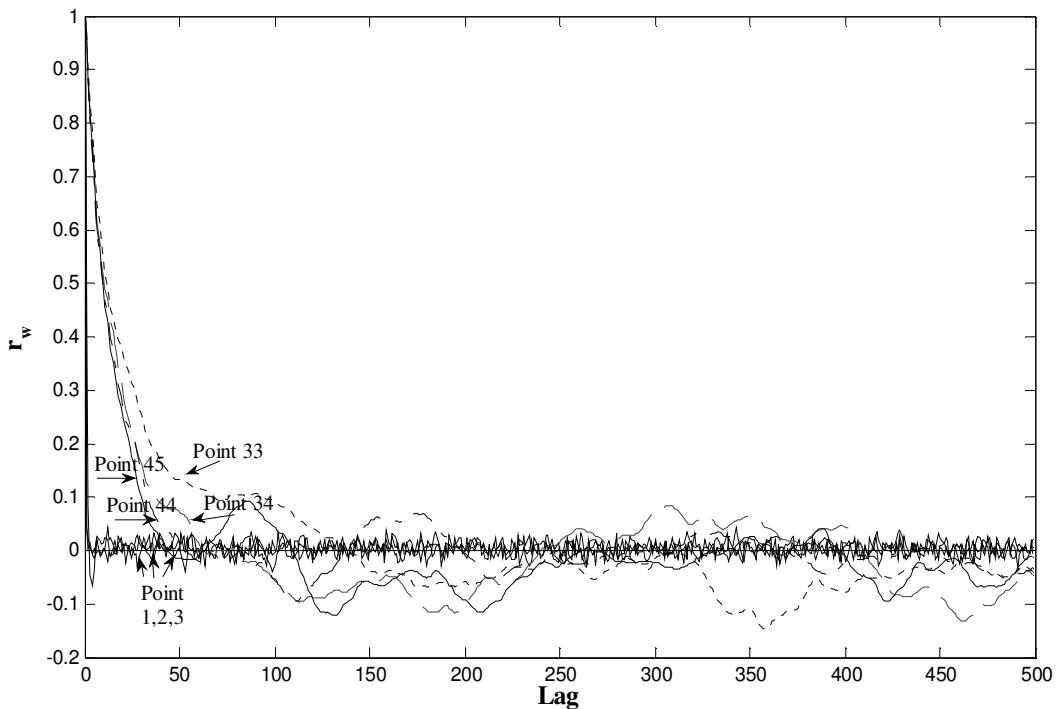


**Figure 7.** Autocorrelation coefficients for points 1, 2, 3, 33, 34, 44, 45 for w component.

given for the representative points mentioned although it is evaluated for all the measurement points along the water column.

Points 33, 34 and points 44, 45 are the points at the middle depth and close to the surface, respectively. Autocorrelation functions at points 1 and 2 decayed abruptly. Therefore, vortex structures are small and random very

close to the bed; their distance to the bed is 0.1 and 1 mm; At point 3, the decay rate of the autocorrelation function is smaller compared to that of the points 1 and 2. Periodicity is also observed in the same auto-correlation function. Therefore, we can deduce that organized structures started to emerge at point 3 which is 1.8 mm apart from the bed. Towards the vertical direction, more

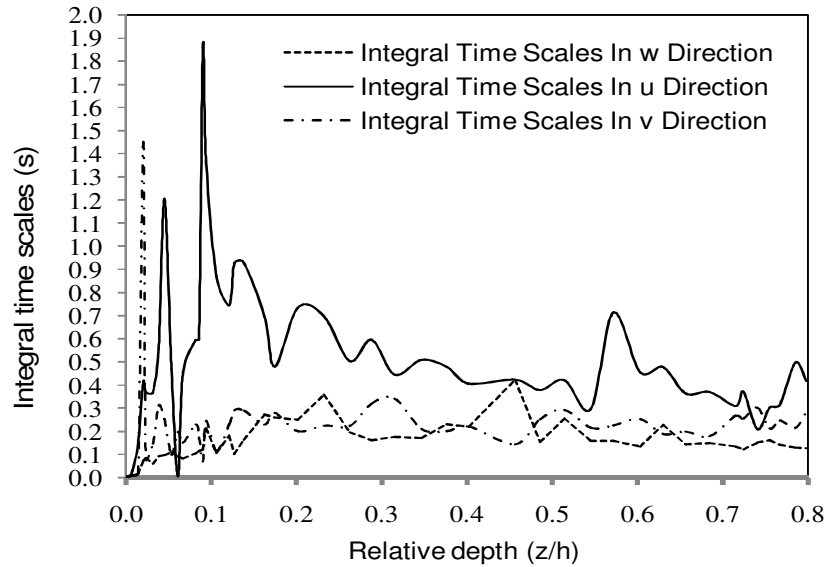


**Figure 8.** Distribution of integral time scales along water depth.

developed mature, organized structures are present as the autocorrelation functions decay much later at points 33, 34, 44 and 45 than point 3. Points 33 and 34 are in the middle of the channel depth whereas points 44, 45 are very close to the surface. If we compare Figures 5 to 7 for each velocity components more organized structures are observed in Figure 5 showing x component of velocity direction. In Figure 6 for v component as seen from the Figure, life time of fluctuating velocities is very short in the vertical plane transverse to the flow. In Figure 6 especially for point 2, remarkable periodicity is observed; this is attributed to the periodic secondary currents.

Using autocorrelation functions for each velocity components, integral time scale for each component can be calculated by evaluating the area under the autocorrelation function, by integrating the autocorrelation function numerically from zero lag to the first zero crossing using Equation 8.

$$T_u = \int_0^t r_{uu}(\Delta t) dt \quad (8)$$

$T$  has a physical meaning also for turbulence studies, “ $T$  gives an indication of the temporal scale of turbulent eddies” (Lacey and Roy, 2008).

As seen in the Figure 8, maximum time scale value is 1.86 s and it is detected at the point 10% of the total depth from the bottom wall. The integral time scale plots indicate that close to the bed, the shear in the mean velocity leads to turbulence production, hence the velocity components are very scattered in this region. Above the point where  $h \approx 0.1 h$ , integral time scales in each direction become closer to each other.

According to Yalin (1972), “the largest eddies do not originate in their full size  $\approx h$  (water depth). Rather they are generated near the flow boundaries (that is near the bed) in the case of an open-channel flow, with a size much smaller than  $h$ : The nearer the birth place of an eddy to the bed, the smaller is its initial size in comparison to  $h$ ”. A significant observation that can be made from these analyses is the differences among the magnitudes of the time scales,  $T_u$ ,  $T_v$ ,  $T_w$ . At around 10% depth,  $T_u/T_v$  ratio reaches its maximum value 26 and then drops rapidly reaching to the value of 3 upto relative depth  $z/h = 0.26$  then drops again to 1.5 to 2 s values up to  $y/h = 0.80$ . The fluctuations in x direction reach their maximum values around 10% of relative water depth.

Another important parameter is integral length scale which can be obtained from  $T$  for u component of velocity as seen in Figure 9. Integral length scale is an important parameter in characterizing the structure of turbulence. It is a measure of the longest correlation distance between the flow velocity (or vorticity, etc) at two points in the flow field. Hinze (1975)

$$L = \bar{U}T \quad (9)$$

Integral length scale plots indicate that integral length scale in u direction reaches its maximum value around 10% of water depth, and then start to decrease to 55% of flow depth, then fluctuates. The integral length scale in v and w directions are very small compared to u direction.

### Distribution of turbulent kinetic energy and flux

Turbulent kinetic energy (TKE) per unit volume of fluid in the fluctuating velocity field is

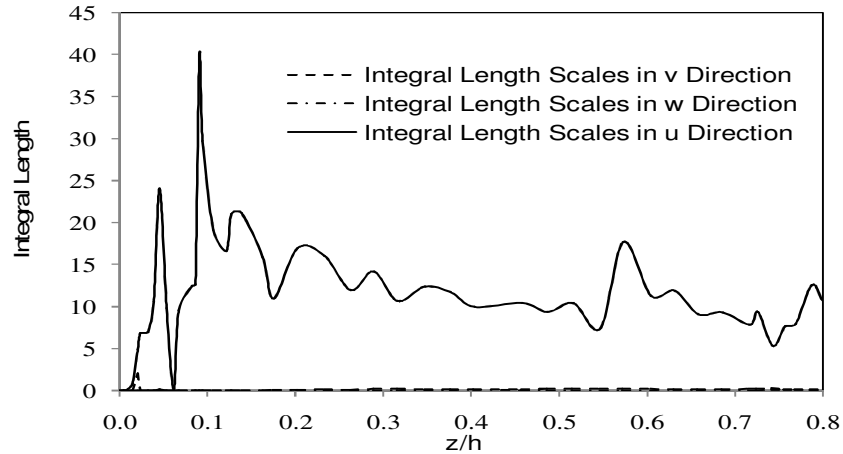


Figure 9. Distribution of integral length scales along flow depth.

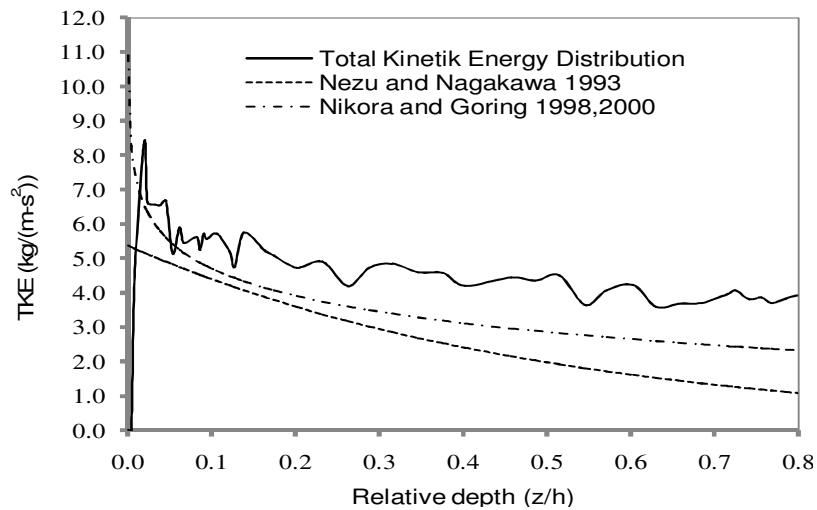


Figure 10. Distribution of total kinetic energy along water depth.

$$TKE = \rho \frac{\overline{u'^2} + \overline{v'^2} + \overline{w'^2}}{2} \tag{10}$$

Using obtained experimental data. The distribution of total turbulent kinetic energy along depth is obtained and shown in Figure 10.

In Figure 10, total TKE reaches its peak at relative depth  $z/h = 0.02$  which is 5 mm above the bed. Then, it starts to decay almost exponentially with fluctuations. Obtained experimental data is compared with two equations that show the total kinetic energy profile. The first equation proposed by Nezu and Nagakawa (1993) and shown as follows:

$$\frac{TKE}{u_*^2} = 4.78 \exp\left(-2 \frac{z}{h}\right) \tag{11}$$

Equation 11 is developed from the  $k-\epsilon$  turbulence model

assuming that turbulent production is balanced by turbulent dissipation. The other equation is proposed by Nikora and Goring (2000).

$$\frac{TKE}{u_*^2} = 1.84 - 1.02 \ln\left(\frac{z}{h}\right) \tag{12}$$

Equation 12 was developed by integrating the velocity spectrum. As seen in the Figure 10, Equation 12 matches to the experimental data better than Equation 11, especially close to the wall. The distribution of turbulent kinetic energy is normalized with the cubic power of shear velocity as shown in Figure 11.

$$\frac{\frac{1}{2} \overline{q^2 w}}{u_*^3} \tag{13}$$

Overall normalized average vertical kinetic energy flux is

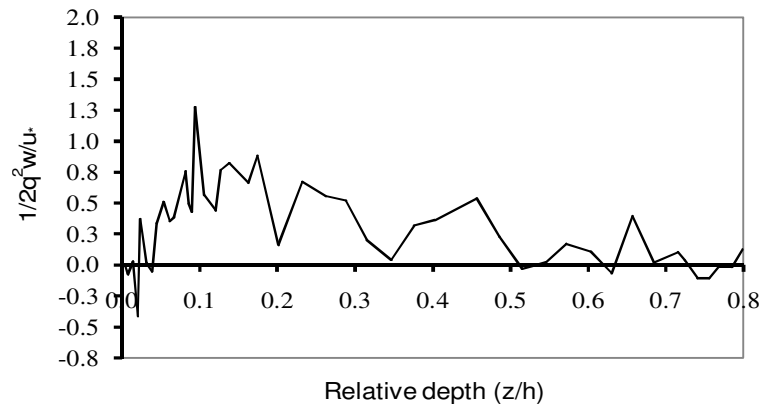


Figure 11. Normalized vertical flux of turbulent kinetic energy.

found as  $\frac{1/2 \overline{q^2 w'}}{u_s^3} = 0.28$ . Lopez and Garcia (1999) performed experiments and they found that near-wall regions of turbulence generation excess, supply turbulent kinetic energy to regions of energy defect near the free surface, through flow regions in local dynamic equilibrium at a normalized vertical flux  $1/2 \overline{q^2 w'} / u_s^3 \approx 0.30$ . This intermediate region seems to extend in the range  $0.15 \leq \eta \leq 0.70$ . In that study in the range  $0.15 \leq z/h \leq 0.70$ , average vertical kinetic energy flux ratio is found as 0.28. This value is almost equal to Lopez and Garcia's (1999) findings. Little difference is attributed to secondary currents.

### Spectral analysis

Spectral analysis helps us to display the distribution of TKE for each velocity component for different frequencies. In spectral analysis, turbulent fluctuations are assumed as superposition of different frequencies. "In most open-channel studies, a three-range model of velocity spectra exist which consists of (1) the production range where spectra behavior has not been identified specifically; (2) the inertial subrange where the large eddies transfer their energy to the smaller eddies. In this subrange auto spectra, follow the "-5/3" law; and (3) the viscous range where the dissipation takes place in small eddies and therefore the decay rate in the energy spectra is higher than the one in the inertial subrange (Nikora and Goring, 2000). In the study, data is sampled with 100 Hz. So Nyquist frequency is 50 Hz. The maximum sampling capacity of the device is 200 Hz. It is observed that at frequencies higher than 100 Hz, very high noise is observed. Therefore, 100 Hz is preferred as sampling frequency. Energy spectrum for each point and for each velocity component is obtained and two representative Figures are prepared as shown in Figures 12 and 13. It is seen as in Figure 12 for point 4 (3.3 mm above the bed)

obtained velocity spectrum very close to the bed contain more noise than the one above the point 33. So the inertial sub-range cannot be clearly observed. However clear from the -5/3 slope of the spectra in Figure 13, which shows the velocity spectra of the inertial sub range can be observed at point which is 11.54 cm above the bed. Additionally -1 slope range is detected within frequency range Nikora (1999) and Nikora and Goring (2000).

### CONCLUSIONS

In this study, data obtained using ADV's analyzed using various approaches. Main findings obtained in the study are given thus

1. As a diverse approach, autocorrelation functions are used to interpret physical characteristics of fluctuating velocity components such as size and life time of eddies along flow depth and important findings are obtained. For a uniform flow, maximum life time and longest approximate dimension of circulating structure is found at 10% of flow depth in the vertical plane parallel to the flow direction. At the depths very close to the bed where vertical gradient of stream wise velocities are large and the life time and fluctuations in u, v and w directions are very small.
2. Integral time scale begins to increase starting from the bed and reaches its maximum value, at 10% of flow depth then starts to decrease.
3. Logarithmic velocity profile is fitted to the obtained data and the best fit is obtained for  $\kappa = 0.4$  and  $A = 6$ .
4. Distribution of turbulent kinetic energy is obtained and it is seen that TKE suddenly increase very close to the bed and it reaches its maximum at relative depth 0.02, then decrease by following a fluctuating trend.
5. Normalized vertical flux of TKE is obtained with well coincidence with the findings of the literature. Distribution of primary Reynolds stress component is checked and

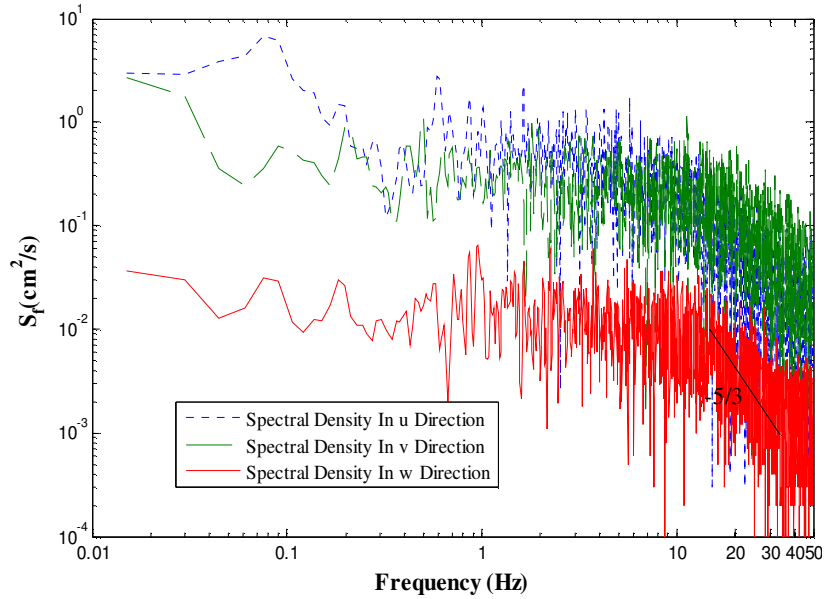


Figure 12. Power spectral density of point 4 for u-v-w velocity components.

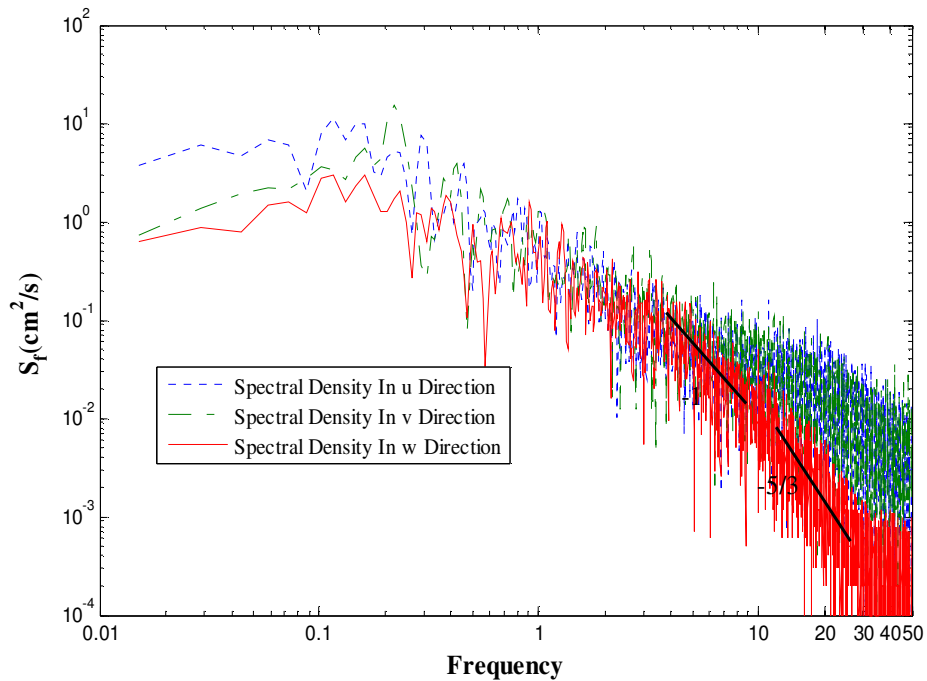


Figure 13. Power spectral density of point 33 for u-v-w velocity components.

seen that it reaches its maximum at relative depth 0.10. 6. Shear velocity is calculated using logarithmic profile approach and Reynolds stress distribution approach. The difference between the two obtained velocity values is 12%.

7. In spectral analysis it is observed that most of the turbulence kinetic energy is concentrated at high period structures (circulations and eddies) as expected. The

spectral density graphs obtained from points which are very close to the bed contain more noise when compared to higher points spectral density graphs. -1 slope is clearly observed before inertial sub-range -5/3 slope.

Future work would probably have to concentrate on measurements taken in the natural environments. Turbulence studies in rivers could shed light to the development and understanding of the subject as one of

the future objectives for this study.

## ACKNOWLEDGEMENT

The author is grateful for the postdoctoral support provided by TUBITAK (Scientific and Technological Research Council of Turkey).

**Notation:** **A**, log-law integration constant; **h**, water depth; **TKE**, turbulent kinetic energy; **U**, Instantaneous velocity;  $\bar{U}$ , mean velocity; **u'**, fluctuating velocity component; **u\***, shear velocity; **z**, distance from bed;  **$\kappa$** , von Karman constant; **r<sub>t</sub>**, autocorrelation coefficient; **s**, turbulence intensity; **s<sup>2</sup>**, variance; **S<sub>f</sub>**, velocity spectral density; **T**, integral time scale; **L**, integral length scale; **N**, number of sampled data; **P**, density of water;  $q^2 = u'^2 + v'^2 + w'^2$ .

## REFERENCES

- Blanckaert K, Lemmin U (2006). Means of Noise Reduction in Acoustic Turbulence Measurements, *J. Hydraulic Res.*, 44(1): 3-17.
- Bombar G, Guney MS, Tayfur G, Elci S (2010). Calculation of the Time-Varying Mean Velocity By Different Methods and Determination of the Turbulence Intensities. *Sci. Res. Essays*, 5(6): 572-581.
- Carollo FG, Ferro V, Termini D (2005). Analyzing Turbulence Intensity in Gravel Bed Channels. *J. Hydraulic Eng.*, 131(12): 1050-1061.
- Cea L, Puertas J, Pena L (2007). Velocity Measurements on Highly Turbulent Free Surface Flow Using ADV. *Experiments in Fluids*, 42(3): 333-348.
- Finelli CM, Hart DD, Fonseca DM (1999). Evaluating the Spatial Resolution of an Acoustic Doppler Velocimeter and the Consequences for Measuring Near-bed Flows. *Limnol. Oceanography*, 44(7): 1793-1801.
- Garcia CM, Cantero MI, Nino Y, Garcia MH (2005). Turbulence Measurements with Acoustic Doppler Velocimeters. *J. Hydraulic Eng.*, 131(12): 1062-1072.
- Goring DG, Nikora VI (2002). Despiking Acoustic Doppler Velocimeter Data. *J. Hydraulic Eng.*, 128(1): 117-126.
- Hinze JO (1975). *Turbulence*, Mc-Graw-Hill.
- Kraus NC, Lohrmann A, Cabrera R (1995). New Acoustic Meter for Measuring 3D Laboratory Flows, *J. Hydraulic Eng.*, 120(3): 406-412.
- Lacey RWJ, Roy AG (2008). Fine-Scale Characterization of the Turbulent Shear Layer of an Instream Pebble Cluster. *J. Hydraulic Eng.*, 134(7): 925-936.
- Lane SN, Biron PM, Bradbrook KF, Butler JB, Chandler JH, Crowell MD, McLelland S, Richards KS, Roy G (1998). Three-dimensional measurement of river channel flow processes using acoustic Doppler Velocimetry. *Earth Surface Processes and Landforms*, 23: 1247-1267.
- Lhermitte R, Lemmin U (1994). Open-Channel Flow and Turbulence Measurement by High-Resolution Doppler Sonar, *J. Atmospheric Oceanic Technol.*, 11(5): 1295-1308.
- Lohrmann A, Cabrera R, Gelfenbaum G, Haines J (1995). Direct Measurements of Reynolds stress with an Acoustic Doppler Velocimeter. In *Proceedings of the Joint Conference on Current Measurement*, St Petersburg, Florida, 7-9 February 205-210.
- Lohrmann A, Cabrera R, Kraus NC (1994). Acoustic-Doppler Velocimeter (ADV) For Laboratory Use. *Proceedings of the Joint Conference on Fundamentals and Advancements in Hydraulic Measurements and Experiments*, Buffalo, New York, 1-5 August 351-365.
- Lopez F, Garcia MH (1999). Wall Similarity in Turbulent Open-Channel Flow. *J. Eng. Mechanics*, 125(7): 789-796.
- Mosalman AR, Mosalman M, Yazdi HM (2011). Equations of Unsteady Flow in Curved Trapezoidal Channels. *Int. J. Phys. Sci.*, 6(4): 671-676.
- Nezu I, Nagakawa H (1993). Turbulence in open-channel Flows. IAHR.
- Nezu I, Rodi W (1986). Open Channel Flow Measurements with a Laser Doppler Anemometer. *J. Hydrol. Eng. Proc. ASCE*, 122: 335-355.
- Nikora V (1999). Origin of the “-1” Spectral Law in Wall-Bounded Turbulence. *Phys. Rev. Lett.*, 83(4): 734-736.
- Nikora V, Goring D (2000). Flow Turbulence over Fixed and Weakly Mobile Gravel Beds. *J. Hydraulic Eng.*, 126 (9): 679-690.
- Nikora VI, Goring DG (2002). Despiking Acoustic Doppler Velocimeter Data. *J. Hydraulic Eng.*, 128(1): 117-126.
- Synder WH, Castro IP (1999). Acoustic Doppler Velocimeter Evaluation in Stratified Towing Tank. *J. Hydraulic Eng.*, 125(6): 595-603.
- Tricito HM, Hotchkiss RH (2005). Unobstructed and Obstructed Turbulent Flow in Gravel Bed Rivers. *J. Hydraulic Eng.*, 131(8): 635-645.
- Voulgaris G, Trowbridge JH (1998). Evaluation of the Acoustic Doppler Velocimeter (ADV) for turbulence Measurements. *J. Atmospheric Oceanic Technol.*, 15: 272-289.
- Wahl TL (2000). Analyzing ADV Data Using WinADV. In *Proceedings of the Joint Conference on Water Resources Engineering and Water Resources Planning & Management*, Minneapolis, Minnesota. July 30- August 2.1-10.
- Yalin MS (1972). *Mechanics of Sediment Transport*. 1<sup>st</sup> Edition. Elsevier. USA.
- Zedel L, Hay AE, Lohrman A (1996). Performance of a Single Beam Pulse to Pulse Coherent Doppler Profiler. *IEEE J. Oceanic Eng.*, 21: 290-297.